




## Article

# Investigation of Chemical, Physical, and Tribological Properties of Pyrolysis Oil Derived from End-of-Life Tires (ELTs) against Conventional Engine Oil

Abdullah A. Alazemi <sup>1,\*</sup> , Abdullah F. Alajmi <sup>1</sup>  and Sultan M. Al-Salem <sup>2</sup> 

<sup>1</sup> Mechanical Engineering Department, Faculty of Engineering and Petroleum, Kuwait University, P.O. Box 5969, Safat 13060, Kuwait; abdullah.alajmi1@ku.edu.kw

<sup>2</sup> Environment & Life Sciences Research Centre, Kuwait Institute for Scientific Research, P.O. Box 24885, Safat 13109, Kuwait; ssalem@kISR.edu.kw

\* Correspondence: a.alazemi@ku.edu.kw

**Abstract:** Over one billion rubber tires are disposed of worldwide annually as a major component of the solid waste stream, posing a significant environmental risk. Therefore, recycling and taking advantage of the rubber component in End-of-Life Tires (ELTs) presents an advantageous opportunity to produce environmentally friendly and cost-effective products. This work studied multiple properties of oil extracted from ELTs using thermal pyrolysis (i.e., pyro-oil) as a potential candidate for industrial lubrication applications. First, pyro-oil was characterized by studying its morphological and chemical properties. Then, rheological studies were conducted to explore the oil properties at different temperatures and shear rates. A tribometer was also used to assess pyro-oil's tribological performance at different temperatures and speeds. Finally, wettability and thermal analyses were performed to understand the wetting and thermal stability properties. The results revealed that pyro-oil has chemical properties similar to conventional engine oil with slightly higher sulfur content. Furthermore, the pyro-oil exhibited lower viscosity and lubrication performance than conventional engine oil, but this difference was smaller at higher temperatures. Thermal stability and wetting properties of pyro-oil were found to be significantly lower than those of conventional engine oil. Based on the properties found and compared with engine oil, pyro-oil presents itself as a suitable liquid lubricant for low-speed, low-load applications operating in temperatures below 61 °C. This work presents a comprehensive study of pyro-oil properties extracted from end-of-life waste tires, offering a feasible route to obtain sustainable and low-cost products.

**Keywords:** recycled tires; pyrolysis process; rheology; tribology; oil thermal stability



**Citation:** Alazemi, A.A.; Alajmi, A.F.; Al-Salem, S.M. Investigation of Chemical, Physical, and Tribological Properties of Pyrolysis Oil Derived from End-of-Life Tires (ELTs) against Conventional Engine Oil. *Lubricants* **2024**, *12*, 188. <https://doi.org/10.3390/lubricants12060188>

Received: 13 April 2024

Revised: 22 May 2024

Accepted: 23 May 2024

Published: 27 May 2024



**Copyright:** © 2024 by the authors. Licensee MDPI, Basel, Switzerland. This article is an open access article distributed under the terms and conditions of the Creative Commons Attribution (CC BY) license (<https://creativecommons.org/licenses/by/4.0/>).

## 1. Introduction

Millions of end-of-life tires (ELTs) are piled up in landfills on an annual basis [1]. The United States Environmental Protection Agency (EPA) states that more than 9,000,000 tons of rubber products were produced, and only 1.67 million tons were recycled in the same year of 2018 [2]. Moreover, ELTs in landfills pose an environmental threat for multiple reasons. Firstly, ELTs can be a fireball hazard with major difficulties in extinguishing them [3]. This was noted in multiple fire incidents in Kuwait, especially in 2012, where some 5 million tires continuously burned for three days [4]. Secondly, rodents, pests, and disease-carrying insects often find waste tires as a favorable breeding environment, leading to the spreading of contagious diseases to humans [5,6]. From an economic point of view, waste tires take up a vast space of valuable land since the void ratio in tires makes up 75% of their volume [7]. Therefore, valorizing ELTs is necessary to reduce the enormous pollution they cause.

The main component of tires is rubber (around 47 wt.%), which is neither fusible nor soluble due to its nature as a chemically cross-linked polymeric matrix that cannot be

remolded into shapes without serious degradation [8,9]. In addition to rubber, tires are made of a complex mixture of carbon black, steel belts and cord, sulfur, zinc oxide, and other components [10]. Due to this complex mixture, ELTs do not degrade naturally, and recycling them by conventional means is laborious [11].

There are multiple ways to recycle waste tires, including retreading, rubber reclaiming, grinding, mechanical lapping, and others [6,12]. However, these recycling processes remain at the physical/mechanical level, such as using rubber after retreading without utilizing its high calorific value ( $32 \text{ MJ Kg}^{-1}$ ) [13]. On the other hand, incineration of ELTs can produce energy but with significant environmental contaminants such as  $\text{CO}_2$ , polycyclic aromatic hydrocarbons (PAH), and sulfur dioxide ( $\text{SO}_2$ ) [14]. Also, economically, the combustion of ELTs does not provide high-end material recovery options and has high capital and operational costs [15].

Pyrolysis provides a feasible solution as a thermochemical conversion (TCC) technique for ELTs, which is based on the dissolution of carbon-based components of tires via heat in inert atmospheres. The products of ELT pyrolysis are gas, oil, and solid char [9]. The gas mainly consists of hydrocarbons (HCs) alongside hydrogen with a high calorific charge and enough energy to be used in industrial applications or to power the pyrolysis process [7]. Al-Qadri et al. [16] demonstrated the techno-economic feasibility of hydrogen production as a clean fuel from waste tires. On the other hand, the char produced by the pyrolysis process contains a very high carbon content with possible usage as carbon black and activated porous carbon particles [6,7], or to be used as a solid fuel source [17]. The main component of the pyrolysis process is the pyro-oil, which accounts for 40–60 wt.% of pyrolysis products. ELT pyro-oil contains aliphatic compounds, aromatic mixtures, impurities (PAH, S, and N mixtures), and more [7]. Some known properties of pyro-oil include having a high calorific value (CV) of about 38 to 45 MJ per Kg, a high density, a small flash point, and a high dynamic viscosity [7,18]. For these reasons, pyrolysis presents a more efficient and environmentally friendly recycling method that has received wide attention [6,9]. Nonetheless, the lubrication and rheological properties of the waste tire pyro-oil are not thoroughly investigated and present a major gap in the technical literature.

Metal lubrication and engine oils (e.g., mineral) have been used in many ways, with applications extending from compressors and compressing systems to engines, turbines, and hydraulics. Tribological and rheological properties constitute the most important function and the best quantitative method to judge their quality [19]. Mineral oils typically contain a complex mixture of HCs and additives. While energy consumption is estimated to be doubled by the year 2030 [20], the economy of oil prices and increase in demand has shown a rapid rise in the interest in 'drop-in' fuels, which constitute similar compositional and chemical properties to conventional fossil fuels [21]. On the one hand, this presents a challenge to producing renewable and sustainable fuels that can replace conventional ones with similar properties and performance in an economically feasible manner. On the other hand, such products should have similar environmental specifications that can meet market expectations. Therefore, the transport sector still shows potential to further investigate the applicability of oils produced from various technologies, especially those that rely on solid waste (SW) and biomass [22–25]. ELTs have presented themselves as a prime example of a special waste category that possesses hazardous potential to the surrounding environment when not dealt with properly [9]. Furthermore, ELTs contain highly energetic substances due to their petrochemical origin [26–29] and have the potential to produce high-quality oils when pyrolysis technology is applied to them [30–37]. Pyrolysis, in particular, has been receiving a lot of attention as a technique to valorize various SW components due to its energy balance and controllable operational parameters, with the potential to produce lucrative products mimicking those of crude oil origin [24]. However, a major gap in the literature exists about the different properties (e.g., rheological and tribological) of pyro-oil obtained from ELTs, which is crucial for determining its appropriate industrial applications.

This research presents a study devoted to determining the different properties of pyro-oil produced from ELTs, including lubrication, rheological, and tribological properties,

and compares them with conventional engine oil. Structural and chemical studies of these recycled materials were achieved by a field emission scanning electron microscope instrument (FE-SEM) and energy-dispersive spectrometry (EDS). Moreover, rheological studies were performed to study the rheological behavior of the pyro-oil at several values of temperature and shear rate. Furthermore, tribological studies were performed on the pyro-oil to evaluate its lubrication performance. Finally, the wetting and thermal properties of the pyro-oil were also investigated.

## 2. Materials and Methods

### 2.1. Samples Acquisition and Materials Acquisition

The samples studied in this work were the pyro-oil samples obtained from the fixed bed pyrolysis of ELTs reclaimed from municipal sources at an average operating temperature of 500 °C, as previously described in [35]. The total oil yield was determined to be around 45% from the treated 200 g feedstock with alumina balls packing. About 90% of the samples (in duplicates) constituted HCs in the range of the C<sub>12</sub>–C<sub>20</sub> compounds. The atomic balance on the reactor system showed that the feedstock contained the following (g): Carbon (C) 164.51, Hydrogen (H<sub>2</sub>) 17.39, Nitrogen (N<sub>2</sub>) 0.33, and Sulfur (S) 6.28. The oil produced contained the following (g): C 80.39, H<sub>2</sub> 13.98, N<sub>2</sub> 0.06, and S 0.30 (further details can be found in [35]). This pyro-oil was compared with virgin commercial engine oil for lubricity and tribology properties as a reference point. The engine oil used was sourced from the Valvoline company (5W-30 Motor Oil), Lexington, KY, USA, with the following constituents as per its materials safety data sheet (MSDS): 36.003% of distillates (petroleum) hydrotreated heavy paraffinic (CAS no. 64742-54-7), 6.88% of hydrotreated light paraffinic distillate (CAS no. 64742-55-8), 6.21% of benzenesulfonic acid, C<sub>10</sub>–C<sub>60</sub>-alkyl derivatives and sodium salts (CAS no. 90194-32-4), and 1.88% of distillates (petroleum) solvent-dewaxed heavy paraffinic (CAS no. 64742-65-0).

### 2.2. Characterization Techniques

#### 2.2.1. Physicochemical Characterization

The oil samples were characterized for their physicochemical properties. The viscosity and rheological properties were measured using an ARES-G2 Rheometer (TA Instruments, New Castle, DE, USA) with a 10 mL sample in each experiment. Viscosity (dynamic) measurement was conducted by performing a temperature ramp starting from 5 °C up to 60 °C. The structure of molecules was determined in the samples by conducting Fourier Transform Infrared Spectroscopy (FTIR) analysis using a model Cary 630 (Agilent, Santa Clara, CA, USA) for the quantitative determination of major and minor atomic elements. The I.R. spectrum obtained for the samples was between wavenumbers (1/λ) ranging from 500 to 4000 cm<sup>-1</sup> following the recent work by Decote et al. [38]. Sequential Wavelength-Dispersive X-ray Fluorescence (WDXRF) was determined using a Rigaku ZSX Primus IV, Tokyo, Japan, to explore the atomic elements in the oil samples quantitatively. In the XRF analysis, a tube above the system is equipped with a powerful 4 kW Rhodium X-ray tube. During the test, a 5 mL liquid sample was placed in a liquid cell container in the instrument.

A light-scattering system, Zetasizer Nano ZS, Malvern, UK, was used for the size measurement and the suspension of particles within the pyro-oil samples. Field Emission Scanning Electron Microscopy (FE-SEM), Model: JSM-7001F, JEOL, Tokyo, Japan, is used to examine the particles' morphology and chemical composition within the pyrolysis oil. Sputter coating with Pt for charging effect was conducted using an auto fine sputter coater (JEOL, Model: JFC-1600, Tokyo, Japan). Carbon, hydrogen, nitrogen, and sulfur content were estimated using a Vario Macro cube analyzer (Elementar, Frankfurt, Germany). The analyzer uses a dynamic combustion process to break down the desired substances into simple compounds. The operating principle of the apparatus is based on burning the sample at an elevated temperature (≥1050 °C). Then, the gaseous product from the sample is directed to the chromatography column by utilizing an inert gas (helium, He) which is used as a carrier. The final products would be in the form of CO<sub>2</sub>, H<sub>2</sub>O, N<sub>2</sub>, and SO<sub>2</sub>.

Finally, the flow enters the gas chromatographic column oven, which ensures uniform and modular temperature, resulting in a complete separation of all elements that are then detected by a thermal conductivity detector (TCD) for C, H, N, and S.

### 2.2.2. Tribological and Wear Scar Studies

An MFT-5000 Multi-Function Tribometer (Rtec instruments, San Jose, CA, USA) was used to conduct the tribological investigations on the oil samples (10 mL) under three temperatures (25, 50, and 75 °C). These temperatures were chosen since most industrial applications involve using oil lubricants in a temperature range from 40 °C to 80 °C [39]. Tribotests were executed according to ASTM-G99 standards [40] using a ball-on-disk arrangement. In all tribotests, a constant normal force of 20 N was applied on a stationary steel ball with a diameter of 9.5 mm, developing a maximum Hertzian contact pressure of 1.3 GPa. This high contact pressure of the ball-on-disk arrangement will guarantee that the oil is tested at the extreme conditions in the boundary and mixed lubrication regimes [41]. A steel disk with a diameter of 50 mm was moving with a rotational speed that ranged from 0 to 1500 rpm. The ball–disk contact in the tribotest occurs at a sliding radius of 12.5 mm. The tribometer was set up for all tests to stabilize the desired temperature in 1 min. Then, the speed was ramped up to 1500 rpm, and the first step in the tribotest started with a duration of 2 min. Afterward, the speed was reduced in multiple steps from high to low in order to examine the lubricant performance in the boundary and mixed lubrication regimes. The total tribotest duration was 74 min. After each test, the wear scars on the disk and ball were scanned by an optical profilometer using magnifications of 10 and 20×. The coefficient of friction (COF) was determined to produce a Stribeck curve to evaluate the lubrication of the pyro-oil in comparison with the engine oil.

### 2.2.3. Wettability Analysis

The wettability analysis for all studied oil samples was conducted via a contact angle goniometer device (DataPhysics Instruments, Filderstadt, Germany, Model: OCA-100-TBU100 TP50) following the procedure previously depicted by Alazmi et al. [42]. Using a square steel substrate with a 5 cm side length, the oil samples' contact angles (CA) under three temperatures (i.e., 25, 50, and 75 °C) were measured through the instrument's software.

### 2.2.4. Thermal Stability Analysis

The thermal stability analysis for the oil samples was conducted according to ASTM-E2550 [43] using a thermogravimetric analyzer (TGA) instrument (METTLER TOLEDO-Model TGA 2, Columbus, OH, USA). The TGA chamber was purged with dry air for one hour before the test. Then, approximately 10 mg of each sample was loaded into a platinum crucible pan with a 70 µL capacity within the TGA instrument. The thermal stability analysis was executed by heating each sample from 25 °C up to 600 °C with a heating rate of 10 °C min<sup>-1</sup> in N<sub>2</sub> gas at a 50 mL min<sup>-1</sup> flow rate.

## 3. Results and Discussion

### 3.1. FTIR Analysis of Oil Samples

The FTIR spectra of the pyro-oil are compiled and depicted in Figure 1, whereby the transmittance of major functional groups is shown in comparison with the results of the virgin engine oil studied. The groups present in the pyro-oil result from the vibration and are displayed as a function of the wavenumbers (frequency, cm<sup>-1</sup>). Theoretically, a near 3000 cm<sup>-1</sup> frequency range indicates an aliphatic alkane (C-H stretching) [44–46], which was quite prominent in our samples with an actual peak at 2726 cm<sup>-1</sup> (Figure 1). Unlike the virgin engine oil, no alkene C-H stretching groups were detected at a wavenumber greater than 3000 cm<sup>-1</sup> for the pyro-oil samples. This was also previously noted by Osayi et al. [47] for two samples extracted from the pyrolysis of natural rubber and used tire pyrolysis oil. The actual peak was detected for the engine oil at about 3700 cm<sup>-1</sup>. Both

CH<sub>2</sub> and CH<sub>3</sub> bending were barely detectable in the studied oil samples. The pyro-oil sample showed a very prominent C=C stretching aromatic ring presence with an intensity (0.18), unlike the engine oil, which was slightly detectable at the same functional group range (Figure 1). Other aromatic rings (C=C) were also detected more prominently between 900 and 690 cm<sup>-1</sup> in the pyro-oil sample, more specifically at peaks almost similar for both samples at a frequency of about 698, 758, 814, 887, and 911 cm<sup>-1</sup>. This shows that the aromaticity of the pyro-oil is higher than that of the conventional engine oil tested. This was also expected with ELT pyro-oils since they are mainly made of monoaromatics (in particular) and aromatic compounds (in general) such as limonene and isoprene [35,48–50]. It is also noteworthy to indicate that, at 1710 cm<sup>-1</sup>, there was a clear peak in the pyro-oil sample associated with carbonyl groups (C=O in stretching) that was not clearly visible in the engine oil. This could be attributed to the oxidation effect taking place with the sample over time and storage. The amide group of aldehydes/ketones (1643 cm<sup>-1</sup>) was visible in both samples but was more prominent in the virgin engine oil (Figure 1). This was a similar case to previous studies conducted on ELT oil samples [46,47]. The engine oil also showed an N-H stretching functional group detected at about 3700 cm<sup>-1</sup> associated with acid chlorides. Acid chlorides (C-Cl, 758 cm<sup>-1</sup>), sulfonamides (N-H, 1515 cm<sup>-1</sup>), and sulfonyl chlorides (S=O, 1377 cm<sup>-1</sup>) were also visible in the pyro-oil samples conforming with previous findings [35]. The dual-peak shape and peaks at near 500 cm<sup>-1</sup> (alcohols, ethers, carboxylic acids, and esters) are commonly noted and associated with aromatics present in various pyro-oils from different feedstock materials, including ELTs [51–53].

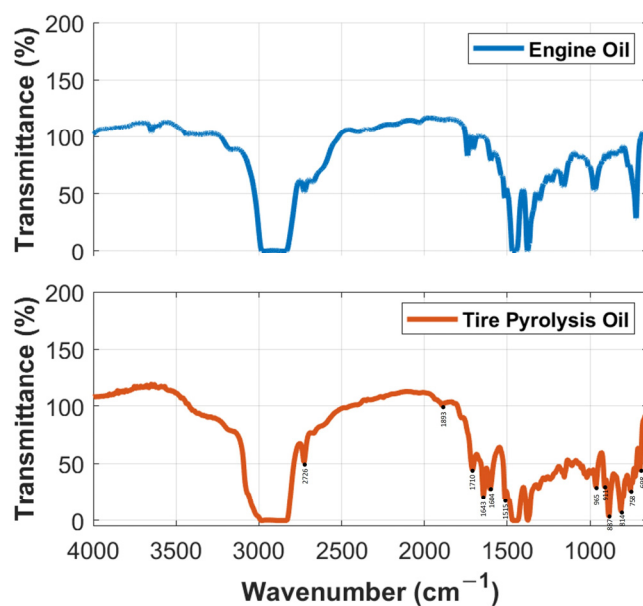


**Figure 1.** FTIR transmittance spectrum for the engine oil (Top) and ELT pyro-oil (Bottom) studied in this work.

### 3.2. Elemental Composition

The elemental composition of engine oil and ELT pyro-oil is shown in the Supplementary Material File for the reader's consideration (Table S1). The ELT pyro-oil sample shows a carbon content of some 47%, conforming with the atomic balance of the sample [35]. It is also of note that minor changes in pyrolysis oils occur over time due to oxidation [54]. The virgin engine oil showed a carbon content of about 50% (Table S1). In terms of the sulfur content, the engine oil contained 0.31%, while the pyro-oil contained 0.72%. The sulfur content agrees with past findings in thermal and catalytic pyrolysis for pyro-oil [48,52] and for used and fresh engine oil [55]. The high sulfur content in pyro-oil compared with engine oil is attributed to the tire's vulcanization process during the manufacturing of tires. The ELT pyro-oil also showed an oxygen content comparable to that of the engine oil



(Table S1), which was determined by subtraction. This indicates that both samples have a similar CV. The XRF analysis also confirms the presence of carbon and sulfur as the most dominant components of the pyro-oil samples investigated (Figure S1). The analysis was quite distinctive in comparison with typical motor oil [56].

ELT pyro-oil contained nano-sized particles, and further investigation to identify their size, shape, and chemical properties was conducted. Static and Dynamic Light Scattering (SDLS) were used to determine the size of the particles in ELT pyro-oil. SDLS results demonstrated that the pyro-oil particles possess sizes that range between 2000 and 6000 nm, with an average particle size of 4548 nm (Figure S2a). To examine the suspension of those particles in the pyro-oil, continuous SDLS measurements were conducted for 12 days (Figure S2b). The results show that the particles can sustain their suspension in the pyro-oil for almost 12 days. It should be noted that the examined sample in the container was stationary during the whole test. Further investigations of the shape and chemical characteristics of the pyro-oil particles were conducted using the FE-SEM instrument. Microscopic images of the pyro-oil particles at various magnifications revealed the irregular shape and micro-sized agglomerated nature of those particles (Figure S3). The chemical composition of the pyro-oil particles was examined using energy-dispersive X-ray spectroscopy (EDS) in the FE-SEM system. The energy-dispersive X-ray examination of those particles shows high carbon content (77.5%) with the presence of sulfur (2.7%) (see Figure S4), which was expected as a result of the tire vulcanization process during manufacturing. It should be noted that the presence of the platinum (Pt) element is discarded since the sample was sputter coated with Pt to visualize the nonconductive pyro-oil particles in the FE-SEM system.

### 3.3. Rheological Analysis

A rheological study of ELT pyro-oil was performed and compared with engine oil at multiple temperatures and shear rates. In the current investigations, the viscosity measurements were performed at different temperatures of 25, 50, and 75 °C and for shear rates of 1 to 100 per second. Figure 2 depicts the viscosity versus the shear rate for pyro-oil and engine oil at 25, 50, and 75 °C. The results revealed that the pyro-oil's viscosity was constant with the variation of shear rate, demonstrating a Newtonian behavior of all samples. Additionally, the viscosity of the pyro-oil was one order of magnitude lower than that of engine oil.

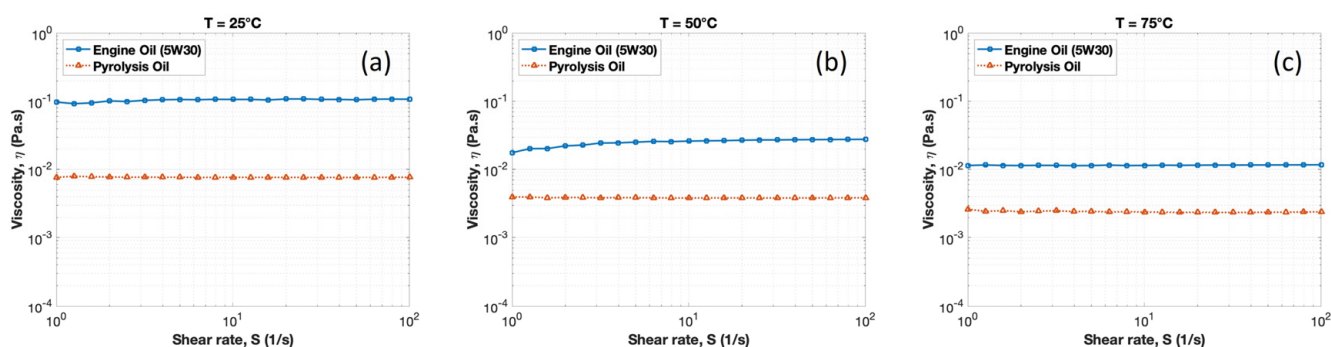


**Figure 2.** Viscosity versus shear rate for pyro-oil and engine oil at different temperatures of (a) 25 °C, (b) 50 °C, and (c) 75 °C.

Further rheological investigations were conducted to examine the variation of shear stress comparatively against the shear rate at different values of temperature. The results revealed that the shear stress was linearly changing with the shear rate for both oil samples and at all temperatures (Figure S5). The pyro-oil had a lower shear stress compared with the engine oil sample at all temperatures and shear rates. However, the difference between the rheological behavior of the pyro-oil and engine oil decreases with the increase in temperature. The variation of the viscosity with temperature was performed for both

oil samples in a temperature range from 5 °C to 60 °C (Figure 3). It can be seen that the pyro-oil viscosity possesses a lower viscosity compared with engine oil at all temperatures. Furthermore, the viscosity of pyro-oil at high temperatures was unstable due to the presence of solid nanoparticles observed in the FE-SEM analysis. The viscosity property is an essential property of oil lubricants since it determines the load-carrying capacity and frictional shear losses within the lubrication system. The obtained rheological results clearly demonstrate that pyro-oil has a lower viscosity property of nearly one order of magnitude than engine oil. Therefore, from the rheological study, it can be concluded that pyro-oil can be utilized in industrial systems that involve low-load applications.

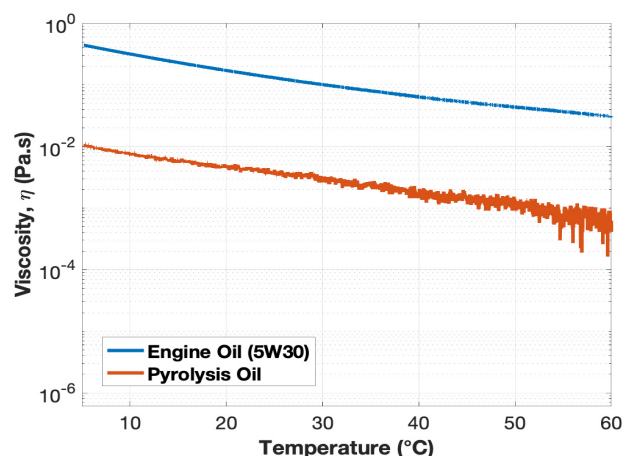


**Figure 3.** Viscosity versus temperature for pyro-oil and engine oil.

### 3.4. Tribological Analysis

A tribological investigation of ELT pyro-oil was conducted and compared with the virgin engine oil at different temperatures. In the current study, all oil samples were examined at different speeds and temperatures to fully understand the lubrication performance of the ELT pyro-oil compared with the engine oil. Figure 4 depicts the variation of the coefficient of friction of all samples with rotational speed at different temperatures. It was noted that the COF for both oil samples decreases with the increase in speed, indicating that the oil is operating in the mixed lubrication regime. Furthermore, the COFs of both oil samples were very close to each other, with a maximum difference that occurs at the highest speed of 1500 rpm (Figure 4). At 25 °C, the COF at 1500 rpm for the engine oil was lower than the pyro-oil by 25%; at 50 °C, the COF at 1500 rpm for the engine oil was lower than the pyro-oil by 20%. The COF at 1500 rpm for the engine oil at 75 °C was lower than the pyro-oil by 36%. The obtained results demonstrate that the pyro-oil has slightly higher friction behavior than the engine oil at high speeds and all temperatures.

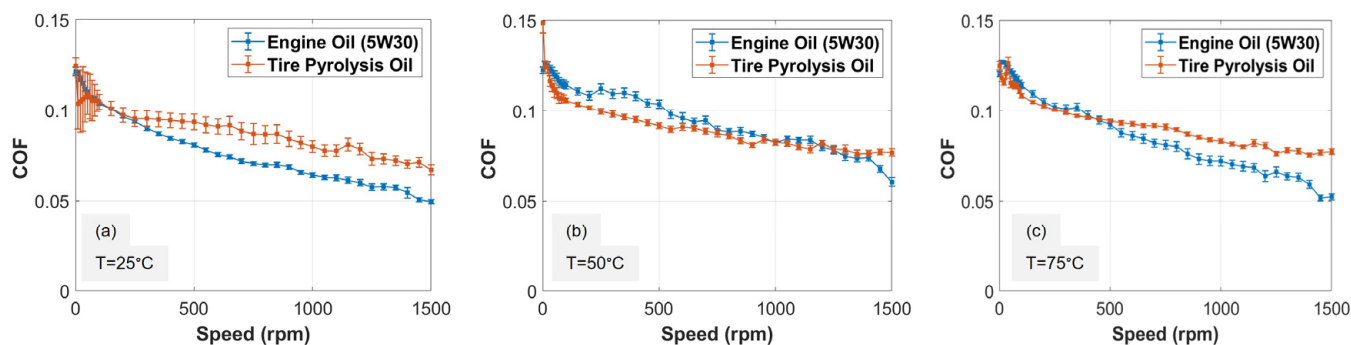


**Figure 4.** COF versus speed for pyro-oil and engine oil at different temperatures of (a) 25 °C, (b) 50 °C, and (c) 75 °C.

Wear analysis was performed on the ball and disk specimens after each tribotest to compare the lubrication performance of the examined oil samples. Figure 5a presents wear scars on the ball specimen after the tribotest at 25 °C temperature for engine oil and pyro-oil. It is clear that the ball wear scar on the engine oil was smaller than the pyro-oil at a temperature of 25 °C. Figure 5b,c present wear scars on the ball specimen after the tribotest at 50 °C and 75 °C temperatures, respectively. The ball wear scars were almost identical for both examined oil samples at 50 °C and 75 °C temperatures. The wear scar diameter of each ball specimen was measured using the optical profilometer, and the wear volume loss was calculated according to the ASTM-G99 standard. The wear results obtained from the ball specimen after tribotests for pyro-oil and engine oil samples at different temperatures are presented in Figure S6. Both oil samples had similar wear behavior at 50 °C and 75 °C temperatures. However, at 25 °C temperature, the engine oil had a wear scar diameter of 295  $\mu\text{m}$  while the pyro-oil had a wear scar diameter of 345  $\mu\text{m}$ . Moreover, the wear volume loss from the engine oil sample was lower than the pyro-oil by 47% at 25 °C. Figure 6 presents wear scars on the disk specimen after the tribotest at 25 °C, 50 °C, and 75 °C temperatures. It is noticeable that the pyro-oil had a wider disk wear scar compared with the engine oil after the tribotest at 25 °C (Figure 6a). However, the disk wear scars were nearly identical for all examined oil samples after tribotests at 50 °C and 75 °C temperatures. Further analysis of the disk wear scar depth was performed by inspecting a line profile perpendicular to the wear scar after the tribotest for both oil samples and at different temperatures (Figure S7). The results show that the wear scars on the disk were shallow, with a depth of less than 0.1  $\mu\text{m}$  for all oil samples and at different temperatures. The friction and wear results obtained from the tribological study clearly indicate that the pyro-oil has a similar lubrication performance compared with the engine oil, particularly at low speeds and higher temperatures.

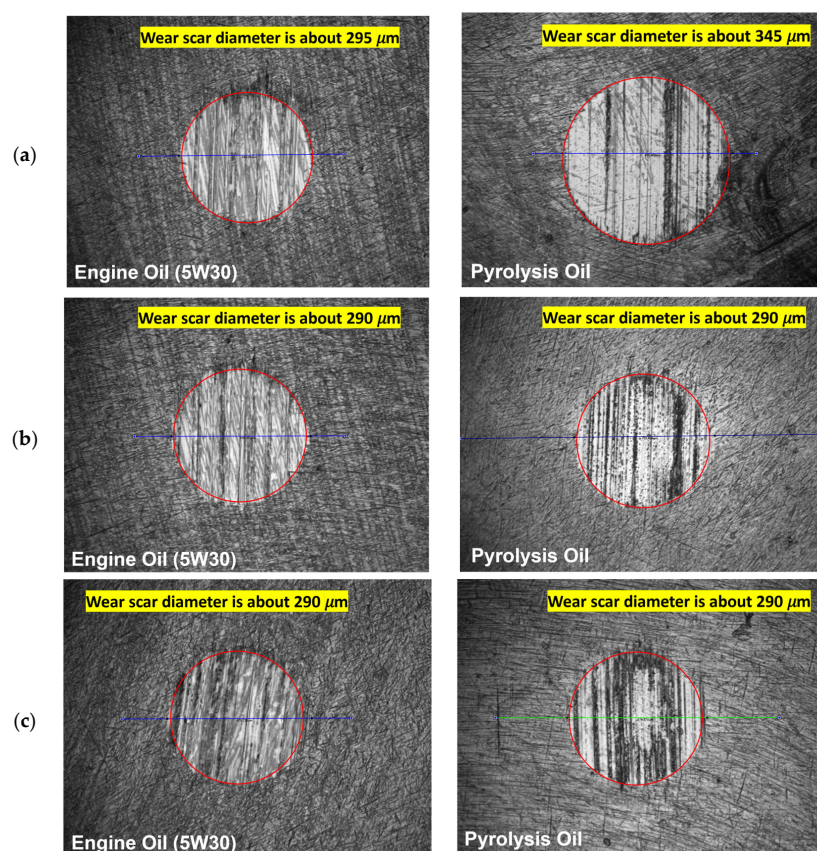


**Figure 5.** Wear scars on the ball specimen for engine oil and pyro-oil after tribotest at (a) 25 °C, (b) 50 °C, and (c) 75 °C temperature. The circle in each figure represents wear scar area.



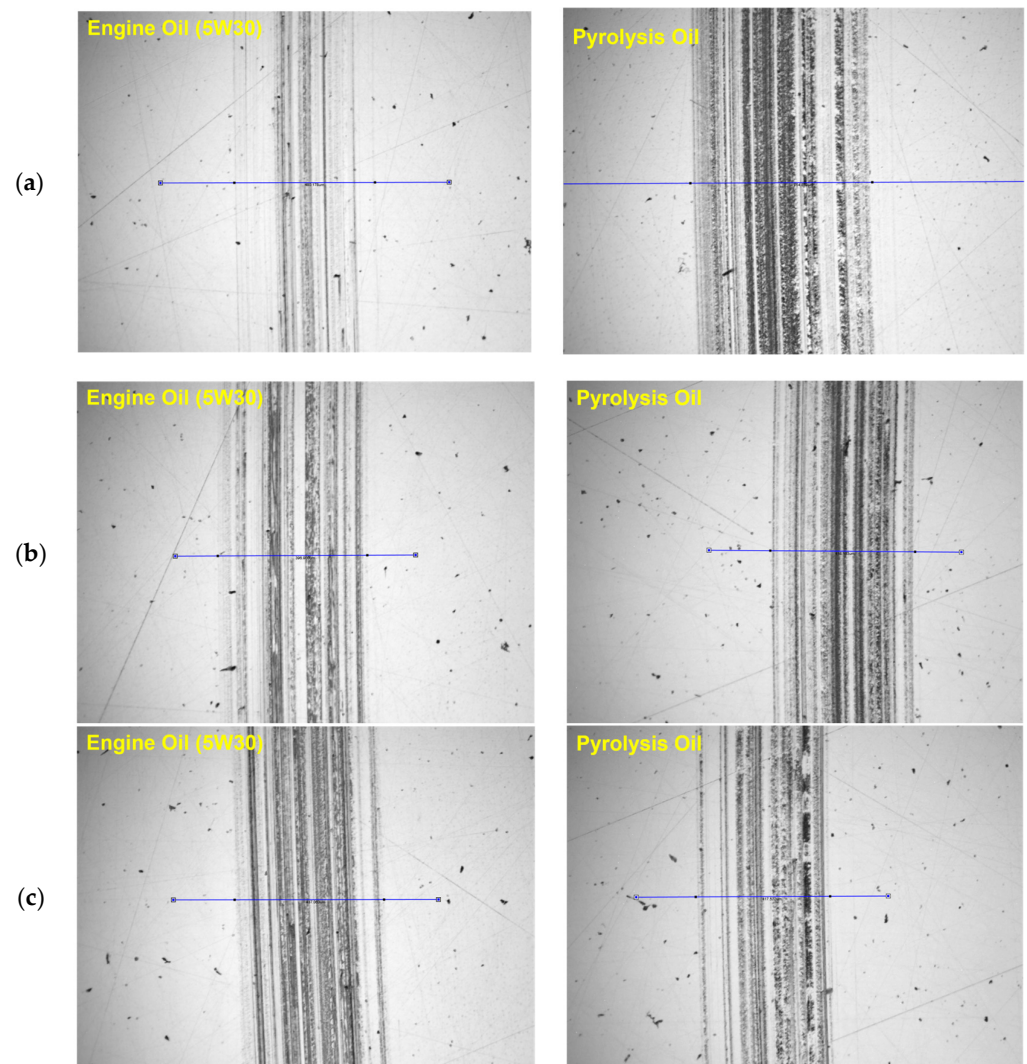


**Figure 6.** Wear scars on the disk specimen for engine oil and pyro-oil after tribotest at (a) 25 °C, (b) 50 °C, and (c) 75 °C temperature.

### 3.5. Regression Analysis of Tribological Data

Examining the experimental results of the tribotests shown in the previous section, a second-order polynomial (data specific regression) model has been developed to describe the coefficient of friction (COF) as a function of (a) RPM ranging from 0 to 1500 and (b) temperature ranging from 25 °C to 75 °C, as follows:

$$\text{Coefficient of Friction (COF)} = 0.104 - (4.7 \times 10^{-5}) \times \text{RPM} + (3.18 \times 10^{-4}) \times \text{Temperature} - (6.51 \times 10^{-8}) \times \text{RPM} \times \text{Temperature} + (1.6 \times 10^{-8}) \times \text{RPM}^2 - (1.82 \times 10^{-6}) \times \text{Temperature}^2 \quad (1)$$

The model's fitness in the previous Equation (1), to the experimental data, has been investigated as shown in Table S2 for the fit statistics. With a regression coefficient ( $R^2$ ) value of 0.915, an adjusted  $R^2$  value of 0.911, and an adequate precision value of around 43, it can be safely assumed that this model shows an excellent fit for the experimental data. The model has been used to generate a 3D surface figure that relates the COF with RPM and operating temperatures, as shown in Figure 7. It can be seen from the generated figure that the experimental data (shown in pink and red dots) below and above the predicted values by the model, which is represented by the surface. For all tested temperatures, the figure shows that the COF decreases with the increase in the RPM, in agreement with the results of the previous sections. Furthermore, it can be noticed from Figure 7 that the operating temperature has a minimal effect on the COF.

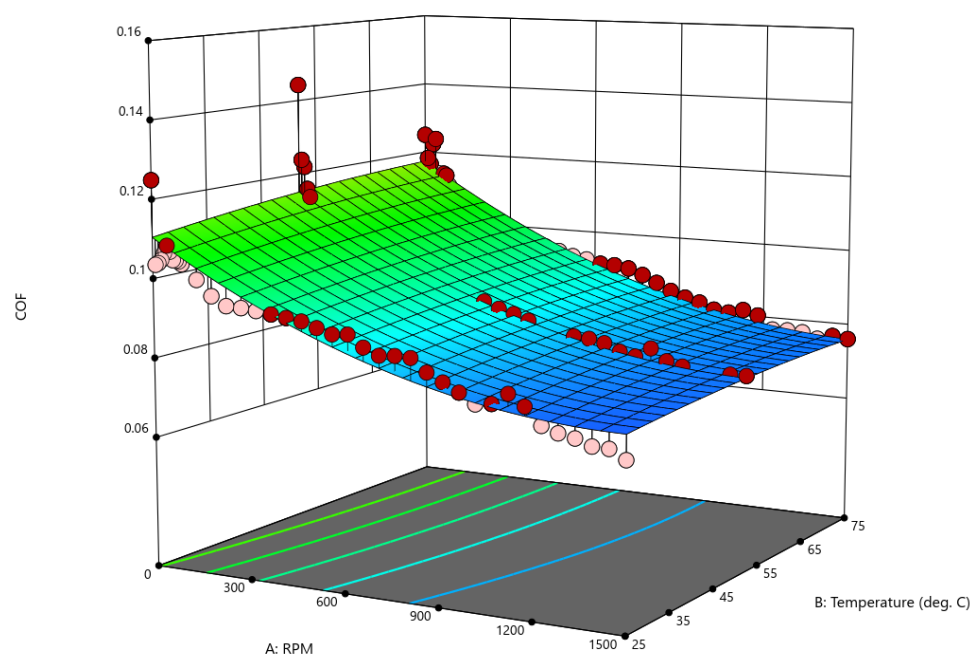


**Figure 7.** COF versus speed and pyro-oil percent at different temperatures. The surface represents the predicted values by the model. Pink and red dots represent the experimental data.

The Analysis of Variance (ANOVA) test works by comparing the means of three or more samples/groups to determine if a significant difference exists between them. An ANOVA test has been conducted to test the significance of the model proposed and the significance of the variables used. More details on how to conduct and interpret the results of the ANOVA test can be found in [57]. The results of the ANOVA test can be summed as (a) the used model is statistically significant in presenting the experimental data, and (b) the RPM and temperature have a statistically significant influence on the value of the coefficient of friction.

### 3.6. Wettability and Thermal Stability

The wetting property of oil lubricants on metal surfaces has a major influence on every tribological system. The existing engine oil lubricants are, in general, petroleum or mineral oils that are prepared with various additives to enhance the oil's lubrication performance. Alterations of engine oils in the past have been performed to attain the best wetting performance on metal surfaces [42]. This section shows the wettability analysis of ELT pyro-oil at different temperatures and compares it with engine oil. The wettability analysis typically includes the measurement of contact angle (CA) as the key parameter, which identifies the wetting level during liquid–solid interaction. All the tested samples demonstrated well-structured drops in CA at different temperatures of 25, 50, and 75 °C (see Figure 8). Figure 9 shows the CA values of pyro-oil and engine oil versus temperature, and it can be seen that the pyro-oil has lower CA values compared with the engine oil. Increasing temperature resulted in a slight increase in the CA value for all oil samples. The lower CA values for the pyro-oil compared with the engine oil can be attributed to the existence of solid nanoparticles, as demonstrated in the FE-SEM analysis. The wide spread of those nanoparticles in the pyro-oil could lead to filling the irregularities on the surface of the metal substrate, resulting in a smoother surface and consequently increasing the wettability and hydrophilic properties of the metal substrate. Furthermore, the presence of these solid nanoparticles leads to increased adhesion between the oil–substrate interface, resulting in a further hydrophilic substrate and, therefore, lowering the CA values compared with the reference engine oil.

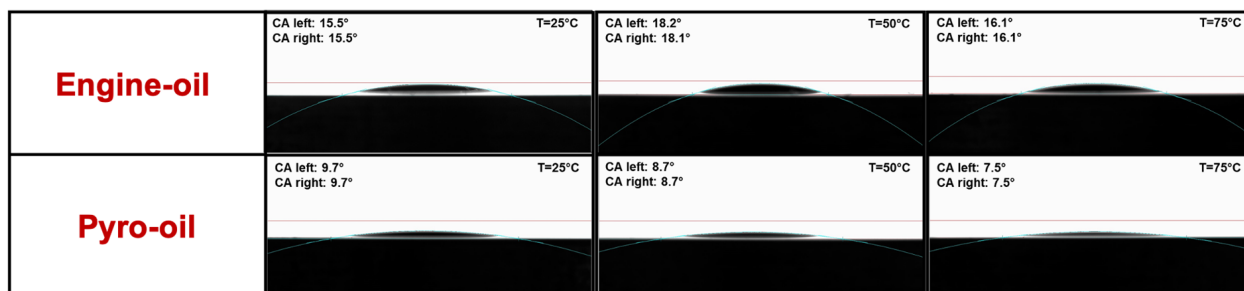


**Figure 8.** Photographs of the drop illustrating the contact angle (CA) at different temperatures for pyro and virgin engine oil.

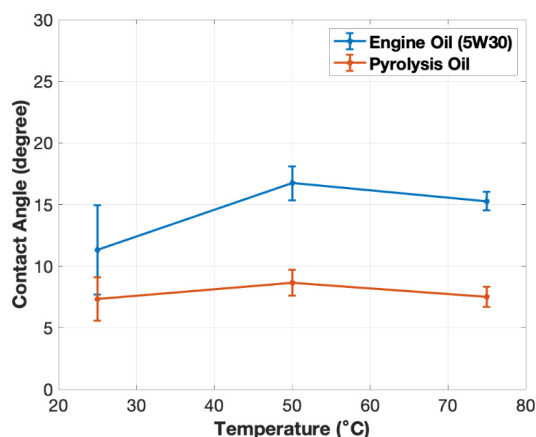


**Figure 9.** Comparison of contact angle values versus temperature for engine oil and pyro-oil.

The thermal stability of ELT pyro-oil was determined and compared with the virgin engine oil by interpreting the TG thermograms (see Figure 10). Thermal stability is a key oil property for oils used as a lubricant operating at elevated temperatures. The thermal stability of oils mostly depends on their chemical structure. The oil's thermal stability is characterized by the onset temperature at which the oil begins to decompose after moisture evaporation. The thermal decomposition involves a mass change, denoted by a change from the initial baseline of the mass [58]. It is clear that the TGA results of both oil samples presented in Figure 10 comprise three phases. In the first phase, only a slight weight decrease of about 1% was observed for both samples. The temperature at which weight loss reaches 1% is called the onset temperature with a post moisture evaporation [59]. In the second phase, reaching up to about 250 °C, a rapid weight loss was observed in both oil samples. A midpoint temperature is identified by the temperature at which the weight loss reaches 50%. The third phase is when the rate of weight loss decreases, reaching a nearly plateau line, and only a few percentages of residual mass remain. It is clear from TGA results that the engine oil has better stability compared with the pyro-oil sample since it started to decompose at an onset temperature of 208 °C. In comparison, the pyro-oil began to decompose at an onset temperature of only 61 °C. Figure 11 represents the first derivative of TG data (DTG) with respect to time for engine oil and pyro-oil. The temperature in the DTG curve at which the mass decomposition rate reaches the maximum point is called the maximum temperature. Afterward, the mass rate decreases until it reaches a plateau line. The DTG curves clearly showed that the engine oil possessed better thermal stability than the pyro-oil sample. Table S3 summarizes the TGA results data for both examined oil samples. The weight loss percentage presented in Table S3 represents the percentage of mass loss by the end of the second phase. The onset decomposition temperature of the engine oil and pyro-oil are 208 °C and 61 °C, respectively. Since most industrial applications involve using oil lubricants in a temperature range from 40 °C to 80 °C [39], it is problematic to use pyro-oil as a lubricant in many industrial applications

that operate at elevated temperatures. However, the pyro-oil is suitable as a liquid lubricant for industrial applications with low operating temperatures.

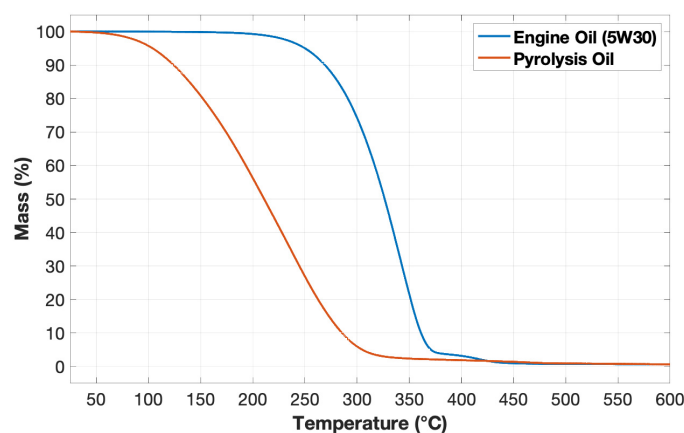


**Figure 10.** Comparison of weight loss profile versus temperature for engine oil and pyro-oil.

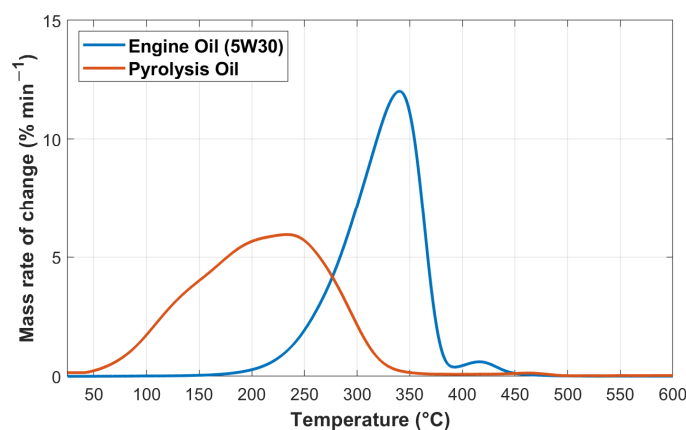


**Figure 11.** Comparison of differential weight loss profile versus temperature for engine oil and pyro-oil.

#### 4. Conclusions

The current research work presented a comprehensive study of the chemical, rheological, tribological, wettability, and thermal stability properties of pyro-oil extracted from recycled used tires. The different properties of the pyro-oil were compared with an engine oil as a reference. The pyro-oil was shown to have similar chemical properties to the engine oil with a slightly higher sulfur content. The ELT pyro-oil was found to contain nano-sized particles with irregular shapes. The obtained rheological results demonstrated that pyro-oil has a lower viscosity property of nearly one order of magnitude compared with engine oil. Tribological analysis was performed to study the friction and wear behavior of the pyro-oil at multiple temperatures. The obtained friction and wear results indicated that the pyro-oil has a lubrication performance nearly similar to engine oil, particularly at low speeds and higher temperatures. Furthermore, a regression model was developed to determine the COF of the pyro-oil at any speed and temperature. Wettability analysis of the pyro-oil on metal surfaces was performed at different temperatures. The pyro-oil was found to have a lower contact angle relative to the engine oil at various temperatures. This can be attributed to the presence of solid nanoparticles in the pyro-oil, leading to a higher adhesion force between the oil–substrate interface, resulting in a more hydrophilic substrate with lower CA values compared with the reference engine oil. Finally, thermal stability analysis was conducted using a TGA instrument for the pyro-oil and engine oil samples. The results revealed that the pyro-oil starts to decompose at an onset temperature of 61 °C, significantly



lower than the engine oil that decomposes at 208 °C. The current study showed that the pyro-oil exhibited lower rheological, wettability, and thermal stability performance compared with the engine oil. However, the chemical and tribological properties of the pyro-oil were comparable to the engine oil. Therefore, the use of pyro-oil as a liquid lubricant can be directed toward industrial applications that involve low speeds, low loads, and operating temperatures less than 61 °C. The use of pyro-oil obtained from recycled tires for industrial lubrication applications can offer a viable use for stockpiled waste tires that possess a serious environmental threat.

**Supplementary Materials:** The following supporting information can be downloaded at: <https://www.mdpi.com/article/10.3390/lubricants12060188/s1>. Figure S1: XRF analysis results (mass %) of the pyro-oil sample; Figure S2: (a) SDLS measurements of intensity versus the range of pyro-oil particles size and (b) SDLS continuous measurements of pyro-oil particles size in oil for 12 days; Figure S3: FE-SEM micro-images of the pyro-oil particles at different magnifications of (a) X250, (b) X500, and (c) X5,000; Figure S4: (a) FE-SEM micrograph and (b) EDS chemical element chart for pyro-oil particles; Figure S5: Shear stress versus shear rate for pyro-oil and engine oil at different temperatures of (a) 25 °C, (b) 50 °C, and (c) 75 °C; Figure S6: (a) Wear scar diameter and (b) wear volume loss from the ball specimen after tribotest at different temperatures for engine oil and pyro-oil; Figure S7: Line profiles across the wear scar on the disk specimen after tribotest at different temperatures for engine oil and pyro-oil; Table S1: Elemental analysis results for oil samples tested; Table S2: Fit statistics of the model; Table S3: Comparison of thermogravimetric analysis data for pyro-oil and engine oil.

**Author Contributions:** All authors contributed to the conceptualization of the study and the development of the methodology. Material preparation, data collection, and analysis were performed by A.A.A. and S.M.A.-S. Statistical analysis was performed by A.F.A. The first draft of the manuscript was written by A.A.A., and it was subsequently revised and edited by all authors. All authors have read and agreed to the published version of the manuscript.

**Funding:** This research was funded by the Research Sector at Kuwait University through research grant number RE01/22.

**Data Availability Statement:** The datasets generated and analyzed during the current study are available from the corresponding author on reasonable request.

**Acknowledgments:** The authors would like to thank the Research Sector at Kuwait University for funding this research project through Research Grant No. RE01/22. The samples were acquired from a prior funded project from the Kuwait Institute for Scientific Research (KISR) through both the Kuwait Foundation for the Advancement of Sciences (KFAS) and the Supreme Council for Planning (Capital Support)—Projects EM085C and P-KISR-06-11. We also would like to acknowledge the help and support of both Hajar Karam and Nasser Al-Sayegh from KISR for their help and support. We gratefully acknowledge the support of Kuwait University General Facilities (Grant No. GE 01/07 and Grant No. GE 03/08).

**Conflicts of Interest:** The authors declare no known competing financial interests or personal relationships that could have appeared to influence the work reported in this article.

## References

1. Revelo, C.F.; Correa, M.; Aguilar, C.; Colorado, H.A. Waste tire rubber powders based composite materials. In *REWAS 2019*; Springer: Berlin/Heidelberg, Germany, 2019; pp. 437–445.
2. EPA. National Overview: Facts and Figures on Materials, Wastes and Recycling. Available online: <https://www.epa.gov/facts-and-figures-about-materials-waste-and-recycling/national-overview-facts-and-figures-materials> (accessed on 30 June 2022).
3. Jang, J.-W.; Yoo, T.-S.; Oh, J.-H.; Iwasaki, I. Discarded tire recycling practices in the United States, Japan and Korea. *Resour. Conserv. Recycl.* **1998**, *22*, 1–14. [[CrossRef](#)]
4. Kerekes, Z.; Lubloy, E.; Kopecsko, K. Behaviour of tyres in fire. *J. Therm. Anal. Calorim.* **2018**, *133*, 279–287. [[CrossRef](#)]
5. Islam, M.R.; Tushar, M.; Haniu, H. Production of liquid fuels and chemicals from pyrolysis of Bangladeshi bicycle/rickshaw tire wastes. *J. Anal. Appl. Pyrolysis* **2008**, *82*, 96–109. [[CrossRef](#)]
6. Sathiskumar, C.; Karthikeyan, S. Recycling of waste tires and its energy storage application of by-products—A review. *Sustain. Mater. Technol.* **2019**, *22*, e00125. [[CrossRef](#)]

7. Zhang, G.; Chen, F.; Zhang, Y.; Zhao, L.; Chen, J.; Cao, L.; Gao, J.; Xu, C. Properties and utilization of waste tire pyrolysis oil: A mini review. *Fuel Process. Technol.* **2021**, *211*, 106582. [[CrossRef](#)]
8. Abdul-Raouf, M.E.; Maysour, N.E.; Abdul-Azim, A.-A.A.; Amin, M.S. Thermochemical recycling of mixture of scrap tyres and waste lubricating oil into high caloric value products. *Energy Convers. Manag.* **2010**, *51*, 1304–1310. [[CrossRef](#)]
9. Williams, P.T. Pyrolysis of waste tyres: A review. *Waste Manag.* **2013**, *33*, 1714–1728. [[CrossRef](#)]
10. Evans, A.; Evans, R. *The Composition of a Tyre: Typical Components*; The Waste & Resources Action Programme: Banbury, UK, 2006; Volume 5.
11. Derakhshan, Z.; Ghaneian, M.T.; Mahvi, A.H.; Conti, G.O.; Faramarzian, M.; Dehghani, M.; Ferrante, M. A new recycling technique for the waste tires reuse. *Environ. Res.* **2017**, *158*, 462–469. [[CrossRef](#)] [[PubMed](#)]
12. Tang, L.; Huang, H. An investigation of sulfur distribution during thermal plasma pyrolysis of used tires. *J. Anal. Appl. Pyrolysis* **2004**, *72*, 35–40. [[CrossRef](#)]
13. Shulman, V.L. Tire recycling. In *Waste*; Academic Press: Cambridge, MA, USA, 2019; pp. 489–515. [[CrossRef](#)]
14. Danon, B.; van der Gryp, P.; Schwarz, C.E.; Gorgens, J.F. A review of dipentene (dl-limonene) production from waste tire pyrolysis. *J. Anal. Appl. Pyrolysis* **2015**, *112*, 1–13. [[CrossRef](#)]
15. Singh, S.; Nimmo, W.; Gibbs, B.; Williams, P. Waste tyre rubber as a secondary fuel for power plants. *Fuel* **2009**, *88*, 2473–2480. [[CrossRef](#)]
16. Al-Qadri, A.A.; Ahmed, U.; Jameel, A.G.A.; Zahid, U.; Ahmad, N.; Shahbaz, M.; Nemitallah, M.A. Technoeconomic Feasibility of Hydrogen Production from Waste Tires with the Control of CO<sub>2</sub> Emissions. *ACS Omega* **2022**, *7*, 48075–48086. [[CrossRef](#)] [[PubMed](#)]
17. Al-Salem, S.M. Pyrolysis of end of life tyres reclaimed from lorry trucks: Part ii—analysis of recovered char. *WIT Trans. Eng. Sci.* **2021**, *133*, 113–117.
18. Al-Salem, S.M. Pyrolysis of end of life tyres reclaimed from lorry trucks: Part i—oil recovery and characterization. *WIT Trans. Eng. Sci.* **2021**, *133*, 107–112.
19. Kupareva, A.; Mäki-Arvela, P.; Murzin, D.Y. Technology for rerefining used lube oils applied in Europe: A review. *J. Chem. Technol. Biotechnol.* **2013**, *88*, 1780–1793. [[CrossRef](#)]
20. Emma, A.F.; Alangar, S.; Yadav, A.K. Extraction and characterization of coffee husk biodiesel and investigation of its effect on performance, combustion, and emission characteristics in a diesel engine. *Energy Convers. Manag.* **2022**, *14*, 100214. [[CrossRef](#)]
21. Januszewicz, K.; Hunicz, J.; Kazimierski, P.; Rybak, A.; Suchocki, T.; Duda, K.; Mikulski, M. An experimental assessment on a diesel engine powered by blends of waste-plastic-derived pyrolysis oil with diesel. *Energy* **2023**, *281*, 128330. [[CrossRef](#)]
22. Han, D.; Ickes, A.M.; Assanis, D.N.; Huang, Z.; Bohac, S.V. Attainment and load extension of high-efficiency premixed low-temperature combustion with edieseline in a compression ignition engine. *Energy Fuels* **2010**, *24*, 3517–3525. [[CrossRef](#)]
23. Kunwer, R.; Ranjit Pasupuleti, S.; Sureshchandra Bhurat, S.; Kumar Gugulothu, S.; Rathore, N. Blending of ethanol with gasoline and diesel fuel—A review. *Mater. Today Proc.* **2022**, *69*, 560–563. [[CrossRef](#)]
24. Al-Salem, S.M.; Antelava, A.; Constantinou, A.; Manos, G.; Dutta, A. A review on thermal and catalytic pyrolysis of plastic solid waste (PSW). *J. Environ. Manag.* **2017**, *197*, 177–198. [[CrossRef](#)]
25. Rajesh, B.; Rajesh, K. Experimental investigation on single cylinder four stroke tri-charged diesel engine using pyrolysis oil at different proportions. *Mater. Today Proc.* **2022**, *52*, 675–682. [[CrossRef](#)]
26. Gehrke, I.; Schläfle, S.; Bertling, R.; Öz, M.; Gregory, K. Review: Mitigation measures to reduce tire and road wear particles. *Sci. Total Environ.* **2023**, *904*, 166537. [[CrossRef](#)]
27. Kole, P.J.; Van Belleghem, F.G.A.J.; Stoorvogel, J.J.; Ragas, A.M.J.; Löhr, A.J. Tyre granulate on the loose; How much escapes the turf? A systematic literature review. *Sci. Total Environ.* **2023**, *903*, 166221. [[CrossRef](#)]
28. Zerin, N.; Rasul, M.; Jahirul, M.; Sayem, A. End-of-life tyre conversion to energy: A review on pyrolysis and activated carbon production processes and their challenges. *Sci. Total Environ.* **2023**, *905*, 166981. [[CrossRef](#)] [[PubMed](#)]
29. Valentini, F.; Pegoretti, A. End-of-life options of tyres. A review. *Adv. Ind. Eng. Polym. Res.* **2022**, *5*, 203–213. [[CrossRef](#)]
30. Tran, T.Q.; Thomas, B.S.; Zhang, W.; Ji, B.; Li, S.; Brand, A.S. A comprehensive review on treatment methods for end-of-life tire rubber used for rubberized cementitious materials. *Constr. Build. Mater.* **2022**, *359*, 129365. [[CrossRef](#)]
31. Antoniou, N.; Stavropoulos, G.; Zabaniotou, A. Activation of end of life tyres pyrolytic char for enhancing viability of pyrolysis—Critical review, analysis and recommendations for a hybrid dual system. *Renew. Sustain. Energy Rev.* **2014**, *39*, 1053–1073. [[CrossRef](#)]
32. Dong, Y.; Zhao, Y.; Hossain, M.U.; He, Y.; Liu, P. Life cycle assessment of vehicle tires: A systematic review. *Clean. Environ. Syst.* **2021**, *2*, 100033. [[CrossRef](#)]
33. Al-Salem, S.; Lettieri, P.; Baeyens, J. Kinetics and product distribution of end of life tyres (ELTs) pyrolysis: A novel approach in polyisoprene and SBR thermal cracking. *J. Hazard. Mater.* **2009**, *172*, 1690–1694. [[CrossRef](#)]
34. Al-Salem, S.; Karam, H.; Al-Qassimi, M. Pyro-gas analysis of fixed bed reactor end of life tyres (ELTs) pyrolysis: A comparative study. *J. Environ. Manag.* **2022**, *320*, 115852. [[CrossRef](#)]
35. Al-Salem, S. Valorisation of End of Life Tyres (ELTs) in a Newly Developed Pyrolysis Fixed-Bed Batch Process. *Process. Saf. Environ. Prot.* **2020**, *138*, 167–175. [[CrossRef](#)]
36. Al-Salem, S. Slow pyrolysis of end of life tyres (ELTs) grades: Effect of temperature on pyro-oil yield and quality. *J. Environ. Manag.* **2022**, *301*, 113863. [[CrossRef](#)] [[PubMed](#)]

37. Antelava, A.; Jablonska, N.; Constantinou, A.; Manos, G.; Salaudeen, S.A.; Dutta, A.; Al-Salem, S.M. Energy Potential of Plastic Waste Valorisation: A Short Comparative Assessment of Pyrolysis vs. Gasification. *Energy Fuels* **2021**, *35*, 3558–3571. [[CrossRef](#)]
38. Decote, P.A.; Negris, L.; Simonassi, P.; Druzian, G.T.; Flores, E.M.; Vicente, M.A.; Santos, M.F. Quality analysis of oil recovered from used locomotive engine oil using ultrasound-assisted solvent extraction. *Chem. Eng. Res. Des.* **2023**, *197*, 603–616. [[CrossRef](#)]
39. Aberoumand, S.; Jafarimoghaddam, A. Experimental study on synthesis, stability, thermal conductivity and viscosity of Cu–engine oil nanofluid. *J. Taiwan Inst. Chem. Eng.* **2017**, *71*, 315–322. [[CrossRef](#)]
40. ASTM G99-17; Standard Test Method for Wear Testing with a Pin-on-Disk Apparatus. ASTM International: West Conshohocken, PA, USA, 2017.
41. Alazemi, A.A.; Etacheri, V.; Dysart, A.D.; Stacke, L.-E.; Pol, V.G.; Sadeghi, F. Ultrasmooth Submicrometer Carbon Spheres as Lubricant Additives for Friction and Wear Reduction. *ACS Appl. Mater. Interfaces* **2015**, *7*, 5514–5521. [[CrossRef](#)]
42. Alazemi, A.A.; Alzubi, F.G.; Alhazza, A.; Dysart, A.; Pol, V.G. Rheological and Wettability Properties of Engine Oil with a Submicron Spherical Carbon Particle Lubricant Mixture. *Int. J. Automot. Technol.* **2020**, *21*, 1475–1482. [[CrossRef](#)]
43. ASTM E2550-17; Standard Test Method for Thermal Stability by Thermogravimetry. ASTM International: West Conshohocken, PA, USA, 2017.
44. Mia, M.; Islam, A.; Rubel, R.I.; Islam, M.R. Fractional Distillation & Characterization of Tire Derived Pyrolysis Oil. *Int. J. Eng. Technol.* **2017**, *3*, 1–10.
45. González, J.F.; Encinar, J.M.; Canito, J.L.; Rodri'guez, J.J. Pyrolysis of automobile tyre waste. Influence of operating variables and kinetics study. *J. Anal. Appl. Pyrolysis* **2001**, *58*, 667–683. [[CrossRef](#)]
46. Williams, P.T.; Besler, S.; Taylor, D.T. The pyrolysis of scrap automotive tyres: The influence of temperature and heating rate on product composition. *Fuel* **1990**, *69*, 1474–1482. [[CrossRef](#)]
47. Osayi, J.I.; Iyuke, S.; Daramola, M.O.; Osifo, P.; Van Der Walt, I.J.; Ogbeide, S.E. Evaluation of pyrolytic oil from used tires and natural rubber (*Hevea brasiliensis*). *Chem. Eng. Commun.* **2018**, *205*, 805–821. [[CrossRef](#)]
48. Jameel, A.G.A.; Alquaity, A.B.; Islam, K.O.; Pasha, A.A.; Khan, S.; Nemitallah, M.A.; Ahmed, U. Pyrolysis and Oxidation of Waste Tire Oil: Analysis of Evolved Gases. *ACS Omega* **2022**, *7*, 21574–21582. [[CrossRef](#)] [[PubMed](#)]
49. Menares, T.; Herrera, J.; Romero, R.; Osorio, P.; Arteaga-Pérez, L.E. Waste Tires Pyrolysis Kinetics and Reaction Mechanisms Explained by TGA and Py-GC/M.S. under Kinetically-Controlled Regime. *Waste Manag.* **2020**, *102*, 21–29. [[CrossRef](#)]
50. Li, D.; Lei, S.; Lin, F.; Zhong, L.; Ma, W.; Chen, G. Study of scrap tires pyrolysis—Products distribution and mechanism. *Energy* **2020**, *213*, 119038. [[CrossRef](#)]
51. Abnisa, F.; Daud, W.M.A.W.; Sahu, J.N. Pyrolysis of mixtures of palm shell and polystyrene: An optional method to produce a high-grade of pyrolysis oil. *Environ. Prog. Sustain. Energy* **2014**, *33*, 1026–1033. [[CrossRef](#)]
52. Chandran, M.; Rajamamundi, P.; Kit, A.C. Tire oil from waste tire scraps using novel catalysts of manufacturing sand (M Sand) and TiO<sub>2</sub>: Production and FTIR analysis. *Energy Sources Part A Recovery Util. Environ. Eff.* **2017**, *39*, 1928–1934. [[CrossRef](#)]
53. Yang, Y.; Zhang, Y.; Omairey, E.; Cai, J.; Gu, F.; Bridgwater, A.V. Intermediate pyrolysis of organic fraction of municipal solid waste and rheological study of the pyrolysis oil for potential use as bio-bitumen. *J. Clean. Prod.* **2018**, *187*, 390–399. [[CrossRef](#)]
54. Stankovikj, F.; Tran, C.-C.; Kaliaguine, S.; Olarte, M.V.; Garcia-Perez, M. Evolution of Functional Groups during Pyrolysis Oil Upgrading. *Energy Fuels* **2017**, *31*, 8300–8316. [[CrossRef](#)]
55. Kupareva, A.; Mäki-Arvela, P.; Grénman, H.; Eränen, K.; Sjöholm, R.; Reunanen, M.; Murzin, D.Y. Chemical Characterization of Lube Oils. *Energy Fuels* **2013**, *27*, 27–34. [[CrossRef](#)]
56. Kadhim, A.; Al-Amiery, A. X-ray Fluorescence of Copper, Nickle and Zinc Nanoparticles in Motor Oil Prepared by Laser Treatment. *J. Adv. Res. Fluid Mech. Therm. Sci.* **2021**, *83*, 178–185. [[CrossRef](#)]
57. Montgomery, D.C. *Design and Analysis of Experiments*; John Wiley & Sons: Hoboken, NJ, USA, 2017.
58. Kalam, M.; Masjuki, H.; Cho, H.M.; Mosarof, M.; Mahmud, I.; Chowdhury, M.A.; Zulkifli, N. Influences of thermal stability, and lubrication performance of biodegradable oil as an engine oil for improving the efficiency of heavy duty diesel engine. *Fuel* **2017**, *196*, 36–46. [[CrossRef](#)]
59. Nik, W.W.; Ani, F.; Masjuki, H. Thermal stability evaluation of palm oil as energy transport media. *Energy Convers. Manag.* **2005**, *46*, 2198–2215. [[CrossRef](#)]

**Disclaimer/Publisher's Note:** The statements, opinions and data contained in all publications are solely those of the individual author(s) and contributor(s) and not of MDPI and/or the editor(s). MDPI and/or the editor(s) disclaim responsibility for any injury to people or property resulting from any ideas, methods, instructions or products referred to in the content.